Title

Performance Comparison of Different Readouts for Position-Sensitive Solid-State Photomultiplier Arrays.

Journal

Biomedical Physics & Engineering Express, 3(4)

ISSN

2057-1976

Authors

Du, Junwei
Schmall, Jeffrey P
Di, Kun
et al.

Publication Date

2017-08-01

DOI

10.1088/2057-1976/aa7c6a

Peer reviewed

HHS Public Access

Author manuscript

Biomed Phys Eng Express. Author manuscript; available in PMC 2018 August 01.

Published in final edited form as:

Biomed Phys Eng Express. 2017 August ; 3(4): . doi:10.1088/2057-1976/aa7c6a.

Performance Comparison of Different Readouts for Position-Sensitive Solid-State Photomultiplier Arrays

Junwei Du[1], **Jeffrey P. Schmall**[1], **Kun Di**[1], **Yongfeng Yang**[1], **Purushottam A. Dokhale**[2], **Kanai S. Shah**[2], and **Simon R. Cherry**[1]

[1]Department of Biomedical Engineering, University of California, Davis, CA 95616 USA

[2]Radiation Monitoring Devices Inc., Watertown, MA 02172, USA

Abstract

A thorough comparison of five different readouts for reading out a 2 × 2 array of 5 mm × 5 mm position-sensitive solid-state photomultipliers (PS-SSPM) was undertaken. The five readouts include reading out the 20 signals (16 position and 4 timing) individually, two signal multiplexing readouts, and two position decoding readouts. Flood histogram quality, signal-to-noise ratio (SNR) and energy resolution were compared at different bias voltage (27.0 V to 32.0 V, at 0.5 V intervals) and at a fixed temperature of 0 °C by coupling a 6 × 6 array of 1.3 mm × 1.3 mm × 20 mm polished LSO crystals to the center of the PS-SSPM array. The timing resolution was measured at a bias voltage of 31.0 V (optimal bias voltage in terms of flood histogram quality). The best flood histogram quality value and signal-to-noise were 7.3 ± 1.6 and 33.5 ± 3.1, respectively, and were obtained by shaping and digitizing the 16 position signals individually. The capacitive charge-division readout is the simplest readout among the five evaluated but still resulted in good performance with a flood histogram quality value of 3.3 ± 0.4 and a SNR of 18.3 ± 1.3. The average energy resolution and the average timing resolution were 15.2 ± 1.2 % and 8.4 ± 1.6 ns for individual signal readout and 15.9 ± 1.2 % and 8.8 ± 1.3 ns by using the capacitive charge-division readout method. These studies show that for an ultra-high spatial resolution applications using the 2 × 2 PS-SSPM array, reading out the 20 signals individually is necessary; whilst the capacitive charge-division readout is a cost-effective readout for less demanding applications.

Index Terms

PET; position-sensitive solid-state photomultipliers; charge division readout

I. Introduction

TO build high-resolution PET or hybrid MRI-compatible PET scanners (Cherry 2006, Judenhofer *et al* 2013 and Senthamizhchelvan *et al* 2013), silicon photomultipliers (SiPM), which also are referred to as multi-pixel photon counters (MPPCs) or solid state photomultipliers (SSPMs), are the best candidate photodetector at the present (Lewellen 2010, McClish *et al* 2010, Yamamoto *et al* 2011, Dokhale *et al* 2013, Pro *et al* 2013 and Seifert *et al* 2013), because of their insensitivity to magnetic fields, compact size and high gain. Position-sensitive solid-state photomultipliers (PS-SSPMs) are novel devices consisting of internally connected cells giving them position sensing ability in a single

device (McClish *et al* 2010 and Schmall *et al* 2012). Compared to the SiPM pixel array detector (Hirano *et al* 2012, Shimizu *et al* 2013 and Du *et al* 2015), the advantages of these PS-SSPMs are the potential for micro-cell level spatial resolution and the easy readout architecture, which requires only five channels to read out the position information and timing information for each gamma photon interaction (McClish *et al* 2010). The disadvantages are the relatively high dark count which prevents fabrication of very large area continuous devices (Schmall *et al* 2012). In collaboration with RMD (Radiation Monitoring Devices Inc.), a 2 × 2 array of PS-SSPMs has been developed to quadruple the detection area (Schmall *et al* 2012 and Du *et al* 2015). This device can resolve crystal arrays with a pitch size of 0.5 mm or even smaller (Schmall *et al* 2012), and therefore provides outstanding spatial resolution for applications such as small-animal PET. But in their current form, this requires 20 readout channels per cm^2 of detector area if each signal is read out individually, 16 anodes channels that encode the position information and 4 cathode channels for timing information. To reduce the cost and complexity of readout electronics it is common to use readout channel reduction techniques in PET detectors (Siegel *et al* 1996, Wu *et al* 2008, Lau *et al* 2010, Downie *et al* 2013, Goertzen *et al* 2013 and Du *et al* 2015). For this PS-SSPM array, a capacitive charge division readout method was designed and evaluated in our previous work (Du *et al* 2015). This readout reduces the 20 channels to 5 channels and the PS-SSPM array can be treated as a virtual continuous device across the entire 10 mm × 10 mm area. Using the capacitive charge readout method, an LSO array with 0.7 mm pitch size has been resolved.

Although the best performance of the device can be achieved by shaping and digitizing each channel, and this represents the gold standard readout method, it is cumbersome, expensive and difficult to implement at the scanner level. The capacitive charge division method is the simplest method to extract position, energy and timing information from the detector, but the performance is reduced because the noise from the four PS-SSPMs is summed. In this paper, the detailed performance of these two readout methods were compared together with other three readout methods. The readout methods were compared using the same experimental setup. The parameters that were measured were the signal-to-noise ratio (SNR), energy resolution and flood histogram quality for bias voltages ranging from 27.5 V to 32.0 V in 0.5 V intervals. The temperature for these measurements was fixed at 0 °C. The timing resolution for the different readout methods was also studied at a temperature of 0 °C and bias voltage of 31.0 V (the optimal value determined by the flood histogram quality results).

II. Material and Methods

A. PS-SSPM and LYSO arrays

A photograph of the 2 × 2 PS-SSPM arrays is shown in Fig. 1 (a) along with a diagram showing the position and nomenclature of the 16 anode signals in Fig. 1 (b). For each of the PS-SSPMs in the array, there is one common cathode signal for timing, which is not shown. The device was fabricated using a complementary metal oxide semiconductor (CMOS) technology. CMOS processing allows for flexible SiPM designs and potentially would permit the readout electronics, such as our capacitive readout circuit and the pre-amplifier, to be incorporated into the device. The size of micro-cell structure is 30 μm on a 44.3 μm pitch

with a capacitance per micro-cell of 220 pF (Schmall *et al* 2012). The total size of this device is 10.0 mm × 10.0 mm with individual PS-SSPMs measuring 4.9 mm × 4.9 mm, with ~ 0.2 mm of dead space between them. Four independent resistor sheets with 246 ohm resistors were used in the 2 × 2 PS-SSPM arrays, with one resistor sheet for each PS-SSPM in the array.

A 6 × 6 polished LSO array, with a crystal pitch of 1.3 mm and a length of 20 mm, separated by enhanced specular reflector (3M), was used for all measurements. The crystal was coupled to the devices using optical grease (Bicron BC-630, Saint-Gobain) and irradiated using a 50 *u*Ci ^{68}Ge point source, placed 10 mm above the front face of the LSO array. The source was moved for the timing measurement, and was placed centrally between the PS-SSPM array and a PMT reference detector with a center-to-center distance of ~80 mm.

The LSO array, detectors, together with the custom made pre-amplifier boards described below were placed inside of a light tight box connected to ground. The air temperature inside the box was controlled using an air-jet crystal cooler (FTS Systems, Inc) and monitored by a Type K thermocouple (DigiSense, Inc). The probe of the thermocouple was placed less than 10 mm from the detector to ensure an accurate measurement of air temperature around the detector.

B. The five readouts methods

Five different readout circuits were designed to read out the signals from the 2 × 2 PS-SSPM arrays, as shown in Fig. 2. Custom made front-end electronic boards were designed in-house to implement the five readout methods using the same Cremat CR-112 preamplifiers in all cases.

The first readout (M1), shown in Fig. 2(a), treats the 2 × 2 PS-SSPM array as four independent PS-SSPM devices and all 20 signals (16 anode signals for position and 4 cathode signals for timing) were discretely read out and amplified using the typical readout method (McClish *et al* 2010 and Schmall *et al* 2012). The best performance can be achieved at the cost of using 16 channels of ADCs, and 4 constant fraction discriminators (CFDs) and time-to-digital convertors (TDCs). This readout was used as a gold standard readout in this paper.

In the second readout (M2), shown in Fig. 2(b), the 16 anode signals initially were also separately amplified by 16 CR-112s, and then multiplexed based on operational-amplifier (Op-Amp) AD8045s (Analog Devices, Inc.) to reduce the 16 anode signals to 4 signals for digitization. The AD 8045 is an ultra low distortion, low noise, high bandwidth (1G Hz) and high slew rate (1350 V/μs) amplifier with a typical quiescent power consumption of 15 mA. Fig. 3 shows one of the four Op-Amp based multiplexers used to combine four signals to one. The 4 amplified cathode signals were fed into four CFDs and TDCs directly to get the timing information and also generate a trigger ID to indicate which PS-SSPM fired.

The third readout (M3), shown in Fig. 2(c), is an analog position decoding method, which we call the voltage-signal redistribution readout. In this method, the 16 individually amplified anode signals (A1′, …, D4′) were fed into the position decoding circuit shown in

Fig. 4. The position decoding circuit is similar to the capacitive circuit shown in our earlier paper (Du *et al* 2013), but a resistor network and Op-Amps were used to perform the position decoding based on the voltage signals, instead of the current signal in the capacitive network. The relationship between the four final positioning signals A, B, C and D and the 16 amplified anode signals are as below:

$$A = A1' + (B1' + C1' + D1' + A2' + A3' + A4')/2$$

$$B = B2' + (A2' + C2' + D2' + B1' + B3' + B4')/2$$

$$C = C3' + (A3' + B3' + D3' + C1' + C2' + C4')/2$$

$$D = D4' + (A4' + B4' + C4' + D1' + D2' + D3')/2$$

The 4 amplified cathode signals were fed into a multiplexing circuit based on the AD8045 similar to that in Fig. 3 to form one common cathode signal. This method reduces the 16 anode signals to 4 signals and the 4 cathode signals to one signal. Using this method, the 2 × 2 PS-SSPM arrays can be treated as one monolithic device and one global standard Anger logic equation can be used to calculate the gamma interaction position for the whole device.

The fourth readout (M4), shown in Fig. 2(d), uses a capacitor-based multiplexer, similar to the one described in (Lau *et al* 2010). A schematic of one multiplexer unit is shown in Fig. 5. In our application, the capacitor value was set to 440 pF based on our previous study (Du *et al* 2013). In this readout, only four pre-amplifiers are needed for the 16 anode signals, but 4 CFDs and 4 TDCs are still needed to obtain the timing information and identify which PS-SSPM device has fired.

The fifth readout (M5), shown in Fig. 2(e), is a capacitor-based position decoding circuit as described in our previous work (Du *et al* 2013), but summarized briefly here. In this readout, a network of capacitors is used to reduce the 16 anode signals to four signals, and the 4 common cathode signals to one cathode signal. The general structure of M5 is similar to that of M4 (Fig. 4), however capacitors are used to couple the PS-SSPM pins to the amplifiers instead of resistors. The values of the capacitors are 220 pF and 440 pf respectively (Du *et al* 2013). The 2 × 2 PS-SSPM array can then be treated to as a single continuous device and a global positioning algorithm can be used for the whole device.

The gamma photon interaction position and deposited energy were calculated using the following formulas:

$$x = \frac{\left(A_d + B_d\right) - \left(C_d + D_d\right)}{A_d + B_d + C_d + D_d}$$

$$y = \frac{(A_d + D_d) - (B_d + C_d)}{A_d + B_d + C_d + D_d}$$

$$E = A_d + B_d + C_d + D_d$$

A_d, B_d, C_d and D_d are the four digitized signals for each PS-SSPM (in M1, M2 and M4) or the whole PS-SSPM array (M3 and M5)

For all readouts, each PS-SSPM can be powered separately by using four independent power supplies outputting different bias voltage to calibrate the gain difference between the four PS-SSPMs. But as the four PS-SSPMs in the arrays turned out to be very homogenous, to simplify the comparison of different readout and the readout electronics, just one global power supply was used. This power supply was sent to the electronic board but then divided into four independent supplies on board by using four π filters (C-L-C) to isolate any crosstalk effects of the other PS-SSPMs.

C. Electronics and Data analysis

The 16 or 4 pre-amplified position signals from the front-end electronic boards were further amplified and shaped by a CAEN spectroscopy amplifier (N586B, CAEN) before being digitized by a PowerDAQ board (Judenhofer *et al* 2005), which includes eight 14 bit ADCs. Ortec 579 fast filter amplifiers and Ortec 584 CFDs were used on the pre-amplified cathode signals to extract timing information and to provide a trigger signal for the PowerDAQ board.

To compare the flood histogram quality, a crystal look up table was applied to the flood histogram to create individual list mode data for each crystal. Then, a flood histogram quality parameter was calculated by comparing the peak position and the spot width for every pair of adjacent crystals in both the x and y directions in the flood (Fig. 6) using the following function.

$$k_i = \frac{p_2 - p_1}{(w_2 + w_1)/2}$$

where w_i and p_i are the FWHMs and centroids of the x or y projections of the i^{th} crystal. Only adjacent crystals coupled to the same PS-SSPM are analyzed, giving 48 different combinations of crystal pairs over which this analysis was performed. The average of the 48 k_i values was used to represent the flood histogram quality and their standard deviation was used as a measure of how uniform the crystal spot width and spacing was within the flood histogram.

The SNR was measured following the methods described in (Du *et al* 2013). Briefly, the noise was quantified using the FHWM of a Gaussian fit to the noise distribution (summed noise from the four position signals acquired by triggering the PowerDAQ using the internal

trigger generated by the computer clock). The average 511 keV photopeak amplitude of the 36 crystals was treated as the signal. A signal offset correction was performed for each channel by subtracting the peak position of the noise distribution from the signal amplitude. The average SNR was then calculated from these two values, the ratio of the signal amplitude and the noise; the standard deviation of the 36 SNR values also was calculated as a measure of the variability of the SNR.

The energy resolution of each crystal was obtained by fitting the 511 keV photopeak using a Gaussian function and the % FWHM of the photopeak was taken as the energy resolution. The average energy resolution of the 36 crystals was used to compare the energy resolution obtained by different readouts, and the standard deviation of the 36 energy resolutions was used to indicate the energy resolution distribution.

The PS-SSPM timing resolution was measured at a bias voltage of 31.0 V, the optimal value determined by the flood histogram quality results. The reference detector was composed of a Hamamatsu H7546B photomultiplier tube (PMT) coupled to a polished LYSO array. The common anode signal of the H7546B was directly fed into an Ortec 579 fast filter amplifier and an Ortec 584 CFD for timing pick off. The PMT timing trigger was used as the start signal and the delayed PS-SSPM timing trigger was used as the stop signal for a Ortec 566 time-to-amplitude converter (TAC). A crystal look up table was also applied to the flood histogram to create individual timing spectra for each crystal. The average FWHMs of the 36 timing spectra, obtained by a Gaussian fit to the timing spectra of the 36 crystals, was defined as the timing resolution of the detector. The timing resolution was quantified by post processing of the data using a 200 keV lower energy threshold and also with an energy window of 400–650 keV.

III. Results

A. Flood histogram

Fig. 7 shows the flood histograms (top) and flood histogram quality metric, *k*, (bottom) obtained at different bias voltages with the five different readout methods. It is clear that the best flood histograms and flood histogram quality are obtained using M1, the 20-channel readout method. Flood histograms from methods M2 and M4 show similar shape to that from M1, but each nine-crystal group, which were coupled to one PS-SSPM device, are compressed and the spots are larger in extent, which is caused by the summation of noise from the whole device. Flood histograms from methods M3 and M5 also show similar shapes, with the crystals being more evenly distributed across the flood histogram, compared to M2 and M4.

The flood histogram quality metric k provides the following information:

- **a.** k from M1 is significantly better than any other method, and is the best readout to achieve highest performance;
- **b.** k from M2 and M3 is higher than that of M4 and M5 respectively, at the cost of using 16 pre-amplifiers to amplify each output individually;

c. Although k measured from the position multiplexer methods (M2 and M4) is better than that from the position decoding methods (M3 and M5), the range of k range (error bar) of the position multiplexer method is also much larger than that of the position decoding method. A smaller range in k range is preferred, as it means the crystals are more evenly distributed. The lower bound of k, and not the average of k, determines how many additional crystals could be inserted and resolved between two crystal spots in Fig. 7 (a), hence, the position decoding methods (M3 and M5) are the preferred method.

d. Considering the small differences in flood histogram quality and the large reduction in electronics components for M5 in comparison to M3, M5 is likely a good choice in many situations among the four simplified methods.

The flood histogram quality differences were negligible for bias voltages varying between 30.0 V to 31.0V for all the readout methods, with the best values of k being achieved at a bias voltage of 31.0V.

The crystal spots in the flood histograms obtained using M3 and M5 are larger than those obtained using other methods, which is caused by the increased crosstalk among different channels in the analog position decoding method.

B. Signal-to-noise ratio

The SNR versus bias voltage for different readout methods is illustrated in Fig. 8. The SNR increases and then decreases slightly with increasing bias voltage. As expected, best SNR was obtained using method M1 at the cost of more electronics. SNR using the position decoding methods (M3 and M5) are better than those using the multiplexer methods (M2 and M4), and the SNR using M2 and M3 are both better than those using M4 and M5. The best SNR were all obtained at a bias voltage of 31.0V, which also corresponds to the optimal bias voltage for the flood histogram quality metric.

C. Energy resolution

Fig. 9 shows the average energy resolution of the 36 crystals. Overall, the best average energy resolution was obtained by using method M3, followed by that of M1 and M5. The energy resolution using position-decoding methods (M3 and M5) are consistently better than those obtained using multiplexer methods (M2 and M4).

Surprisingly, the best average energy resolution was not obtained by using method M1. To further investigate this, the average energy resolution of the four corner crystals, four inner crystals and four center crystals, as defined in Fig. 10(a), were evaluated separately (Fig. 10(b)). It is important to note that each corner crystal was coupled to the center of one PS-SSPM, while each center crystal was coupled to the corner of the PS-SSPM. The best energy resolution for the corner and inner crystals were actually obtained using M1. However, due to light sharing, the center crystals have signal shared across all four PS-SSPMs, and here the advantages of method M1 disappear because each of the individually amplified signals is relatively small in amplitude and the other method give better energy resolution.

D. Timing resolution

The normalized timing spectra for an individual center, inner and corner crystal obtained using method M5 are shown in Fig. 11 (a). The typical crystal dependent timing shift and timing resolution of the PS-SSPM, due to the resistive readout (Schmall *et al* 2012), is clearly observed. The average timing resolution of the 36 crystals at a bias voltage of 31.0 V is shown in Fig. 11 (b), using a 200 keV lower energy threshold and after post-processing the data with a 400–650 keV energy window. The timing resolutions are comparable using the different readout methods, likely because the values are dominated by the resistive readout of the PS-SSPM and not the noise contributed by the electronic readouts.

IV. Conclusion and Discussion

The 2 × 2 array of PS-SSPMs is targeted for ultra-high resolution small-animal PET applications. To maintain the high resolution at a PET system level, dual-ended readout to obtain depth-of-interaction (DOI) information is needed (Yang *et al* 2008 and Yang *et al* 2011), which requires 40 readout channels per detector module. Although the best flood histogram can be achieved by shaping and digitizing each channel individually, the cost and complexity of the electronics will be significant. One of the advantages of SiPMs relative to APDs are their high gain, which should make it possible to build a PET scanner with low-cost electronics. If large-area, high performance PS-SSPMs cannot fabricated with simple readout, this will likely limit their applications.

In this work, we presented a thorough comparison of five different electronic circuits for reading out the signals from a 2 × 2 array of 5 mm × 5 mm PS-SSPMs by comparing the flood histogram quality, signal-to-noise ratio, energy resolution and timing resolution. The results show that the flood histogram quality and signal-to-noise ratio were degraded using multiplexer readouts or position decoding readouts that reduce the number of readout channels due to the summation of noise from all four PS-SSPMs, compared to readout of the 16 cathode signals individually. Energy resolution obtained by using the position decoding readout and reading out the 16 cathode signals individually are quite comparable, and are better than those achieved using the signal multiplexer readout. The timing resolution ranged from 8.2 ± 1.4 ns to 8.8 ± 1.3 ns for different readouts when a 400 – 650 keV energy windows was applied to each crystal with little dependence on the readout method.

Table I lists the required electronics components and the achieved best performance for the five readout methods. Of the four signal reduction readouts investigated in this paper, the results show that the position decoding readouts (M3 and M5) overall give better performance than the signal multiplexer methods (M2 and M4), especially for the flood histogram and signal-to-noise ratio. Considering the significant reduction of amplifiers (from 25 to 5) required for the capacitive charge-division readout (M5), compared to the voltage-signal redistribution readout (M3), and the minimal performance degradation, the capacitive charge-division readout will be employed in our future development, for example in developing a dual-ended detector with DOI encoding capability. This scheme reduces the number of readout channels for a PET scanner to one fourth of those that would be required for reading out each channel individually.

Acknowledgments

This work was supported by NIH grant R01 CA134632.

References

Cherry SR. Multimodality in vivo imaging systems: Twice the power or double the trouble? Annu Rev Biomed Eng. 2006; 8:35–62. [PubMed: 16834551]

Dokhale P, Schmall J, Stapels C, Christian J, Cherry SR, Squillante MR, Shah KS. Imaging and timing performance of 1cm × 1 cm position-sensitive solid-state photomultiplier. 14th international workshop on radiation imaging detectors. 2013:1–4.

Downie E, Yang X, Peng H. Investigation of analog charge multiplexing schemes for SiPM based PET block detectors. Phys Med Biol. 2013; 58:3943–3964. [PubMed: 23680653]

Du J, Schmall J, Yang Y, Di K, Dokhale P, Shah KS, Cherry SR. A simple capacitive charge-division readout for position-sensitive solid-state photomultiplier array. IEEE Trans Nucl Sci. 2013; 60:3188–3197. [PubMed: 25558081]

Du J, Schmall J, Yang Y, Di K, Roncali E, Pavlov N, Buckley S, Jackson C, Cherry SR. Evaluation of Matrix9 Silicon Photomultiplier Array for Small-Animal PET. Med Phys. 2015; 42:585–599. [PubMed: 25652479]

Goertzen AL, Zhang X, McClarty MM, Berg EJ, Liu C, Kozlowski P, Retière F, Ryner L, Sossi V, Stortz G, Thompson CJ. Design and performance of a resistor multiplexing readout circuit for a SiPM detector. IEEE Trans Nucl Sci. 2013; 60:1541–1549.

Hirano Y, Inadama N, Yoshida E, Nishikido F, Murayama H, Watanabe M, Yamaya T. Potential for reducing the numbers of SiPM readout surfaces of laser-processed X'tal cube PET detectors. Phys Med Biol. 2012; 58:1361–1374.

Judenhofer MS, Cherry SR. Applications for preclinical PET/MRI. Semin Nucl Med. 2013; 43:19–29. [PubMed: 23178086]

Judenhofer M, Pichler B, Cherry SR. Evaluation of high performance data acquisition boards for simultaneous sampling of fast signals from PET detectors. Phys Med Biol. 2005; 50:29–44. [PubMed: 15715420]

Lau F, Vandenbroucke A, Reynolds P, Olcott P, Horowitz M, Levin CS. Analog signal multiplexing for PSAPD-based PET detectors: simulation and experimental validation. Phys Med Biol. 2010; 55:7149–7174. [PubMed: 21081831]

Lewellen T. The challenge of detector designs for PET. Nuclear Medicine and Molecular Imaging. 2010; 195:301–309.

McClish M, Dokhale P, Christian C, Stapels C, Johnson E, Robertson R, Shah KS. Performance measurements of CMOS position sensitive solid-state photomultipliers. IEEE Trans Nucl Sci. 2010; 57:2280–2286.

Pro T, Ferri A, Gola A, Serra N, Tarolli A, Zorzi N, Piemonte C. New developments of near-UV SiPMs at FBK. IEEE Trans Nucl Sci. 2013; 60:2247–2253.

Schmall J, Du J, Yang Y, Dokhale P, McClish M, Shah KS, Cherry SR. Comparison of large-area position-sensitive solid-state photomultipliers for small animal PET. Phys Med Biol. 2012; 57:8119–8134. [PubMed: 23172720]

Seifert S, van der Lei G, van Dam HT, Schaart DR. First characterization of a digital SiPM based time-of-flight PET detector with 1 mm spatial resolution. Phys Med Biol Vol. 2013; 58:3061–3074.

Senthamizhchelvan S, Zaidi H. Novel quantitative techniques in hybrid (PET-MR) imaging of brain tumors. PET Clinics. 2013; 8:219–232. [PubMed: 27157949]

Shimizu K, Uchida H, Sakai K, Hirayanagi M, Nakamura S, Omura T. Development of a multi-pixel photon counter module for positron emission tomography. IEEE Trans Nucl Sci. 2013; 60:1512–1517.

Siegel S, Silverman R, Shao Y, Cherry SR. Simple charge division readouts for imaging scintillator arrays using a multi-channel PMT. IEEE Trans Nucl Sci. 1996; 43:1634–1641.

Wu Y, Catana C, Cherry SR. A multiplexer design for position sensitive avalanche photodiode detector in a PET scanner. IEEE Trans Nucl Sci. 2008; 55:463–468.

Yamamoto S, Watabe T, Watabe H, Aoki M, Sugiyama E, Imaizumi E, Kanai Y, Shimosegawa E, Hatazawa J. Simultaneous imaging using Si-PM-based PET and MRI for development of an integrated PET/MRI system. Phys Med Biol. 2011; 57:N1–N13. [PubMed: 22170810]

Yang Y, Qi J, Wu Y, St James S, Farrell R, Dokhale PA, Shah KS, Cherry SR. Depth of interaction calibration for PET detectors with dual-ended readout by PSAPDs. Phys Med Biol. 2008; 54:433–445. [PubMed: 19098356]

Yang Y, Wu Y, Farrell R, Dokhale P, Shah KS, Cherry SR. Signal and noise properties of position-sensitive avalanche photodiodes. Phys Med Biol. 2011; 56:6327–6336. [PubMed: 21896961]

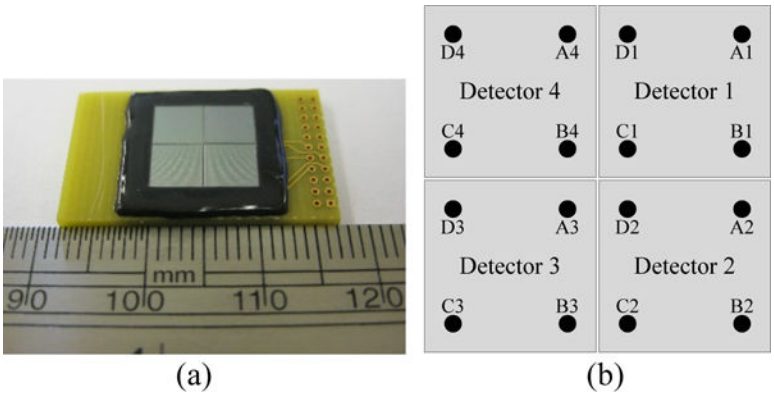

Fig. 1.
(a) Photograph and (b) schematic of the 2 × 2 PS-SSPM arrays.

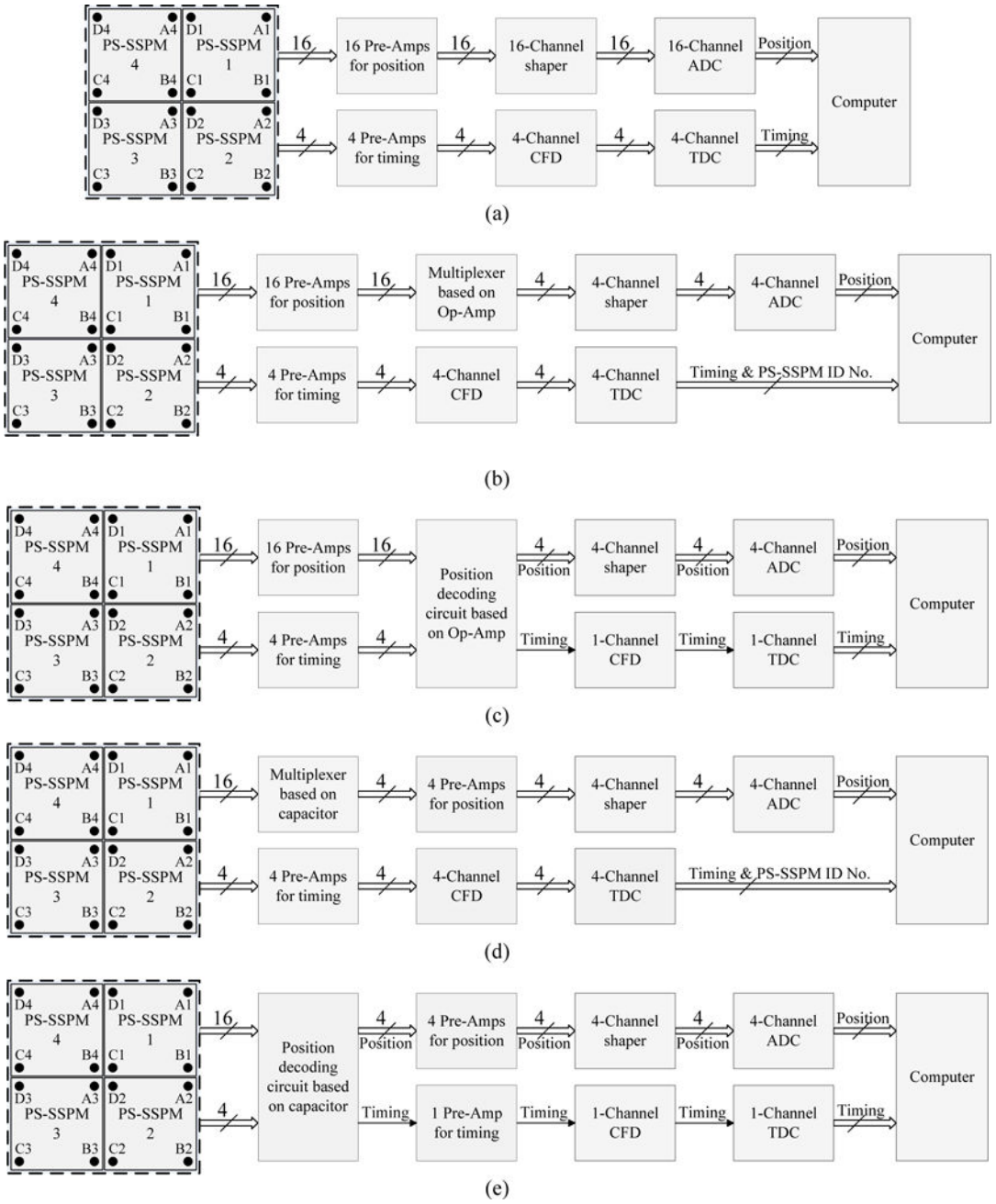

Fig. 2.

(a) 20-channel readout (M1), (b) Op-Amp based multiplexer (M2), (c) Op-Amp based position decoding (M3), (d) capacitor based multiplexer (M4), (e) capacitor based position decoding (M5). From circuit M1 to M5, the electronics become simpler.

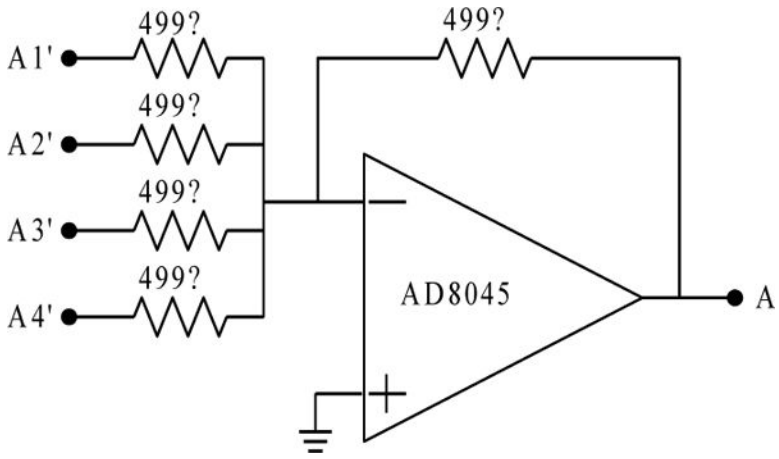

Fig. 3.
OP-Amp based multiplexer.

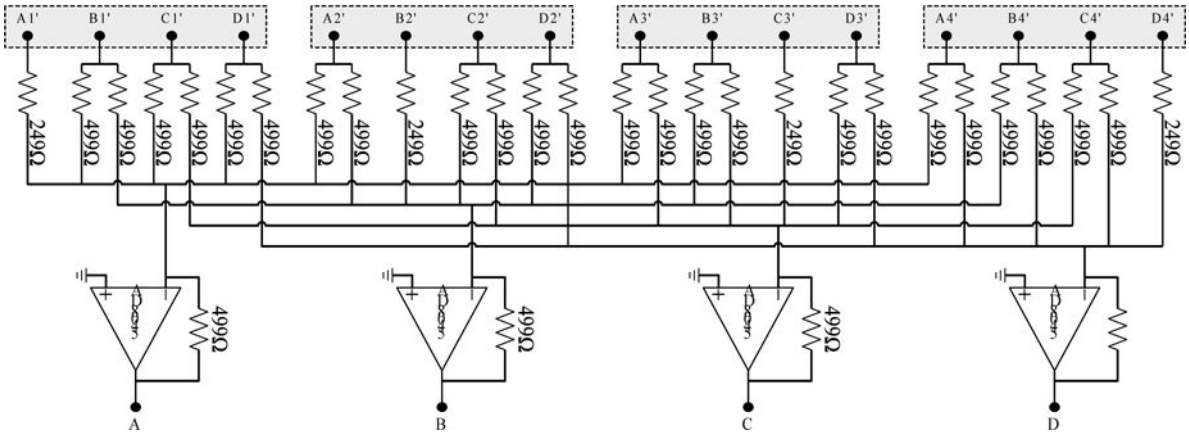

Fig. 4.
Op-Amplifier based position decoding readout used in method M3.

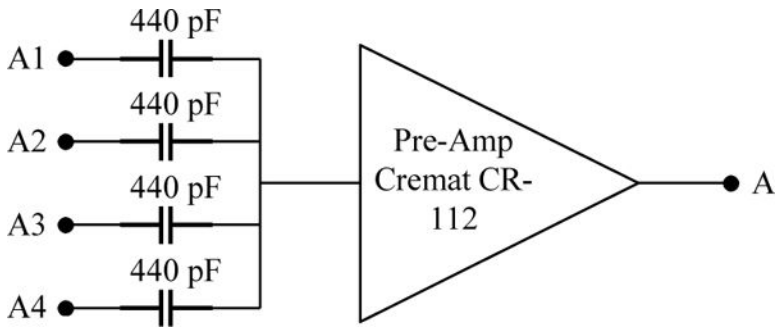

Fig. 5.
Capacitor-based multiplexer.

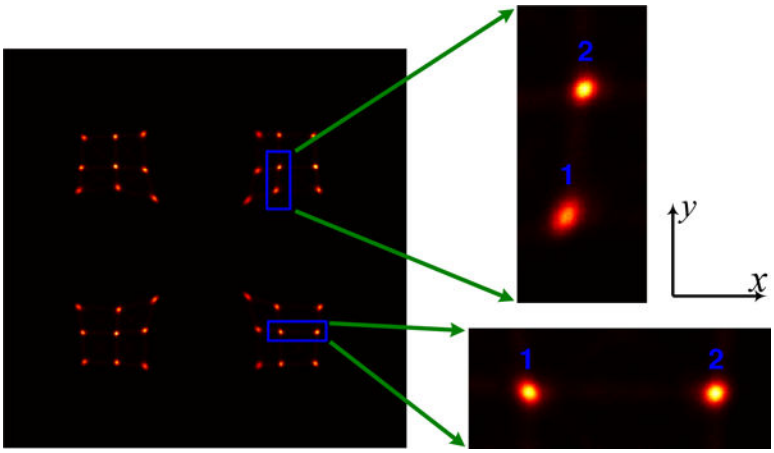

Fig. 6.

Illustration of pairs of adjacent crystals in *x*- and *y*-directions used to determine flood histogram quality using Eq. 2.

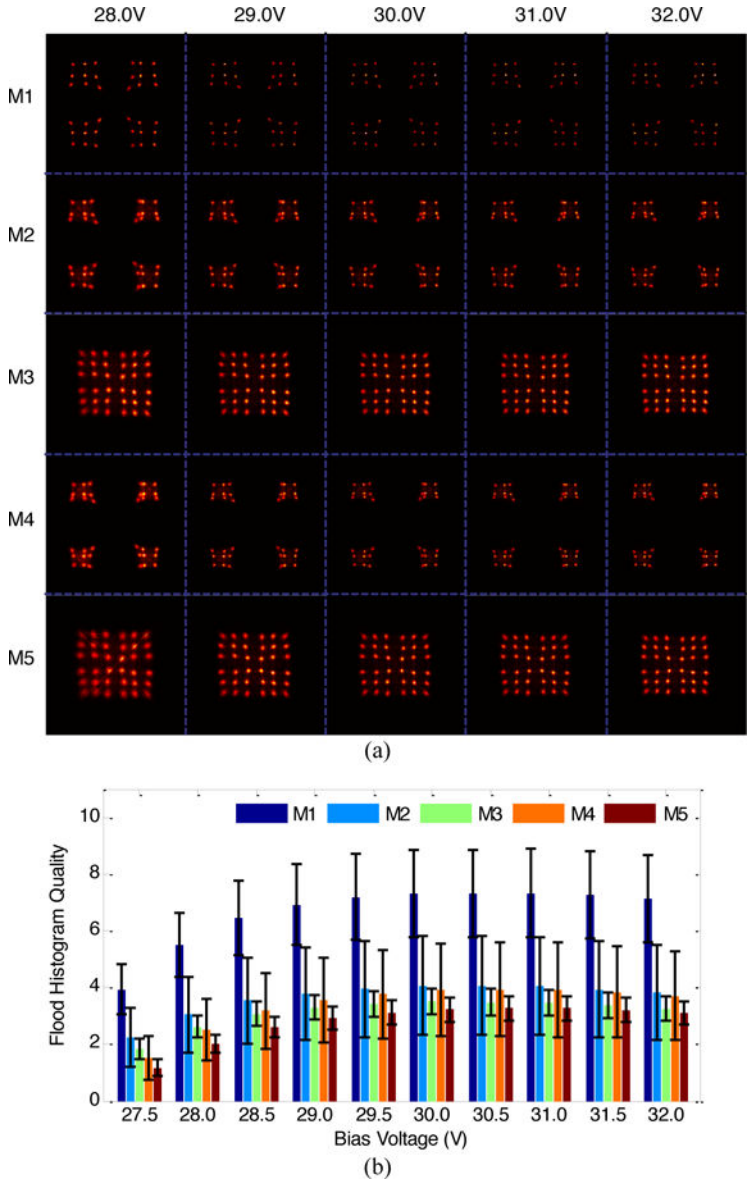

Fig. 7.

(a) Flood histogram and (b) flood histogram quality for the five different readout methods.

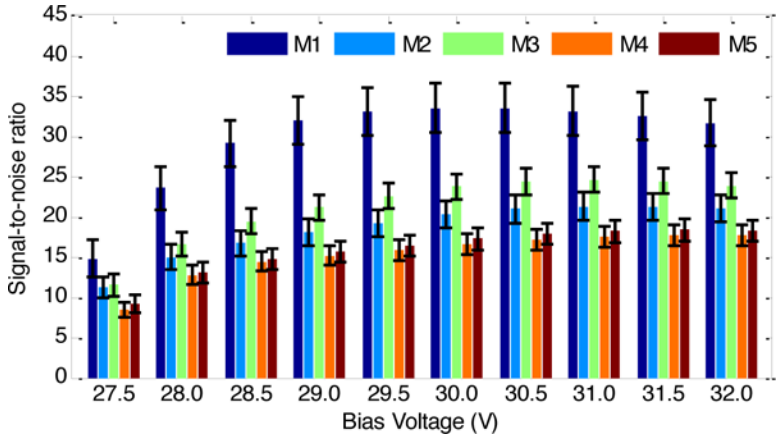

Fig. 8.
SNR versus bias voltage.

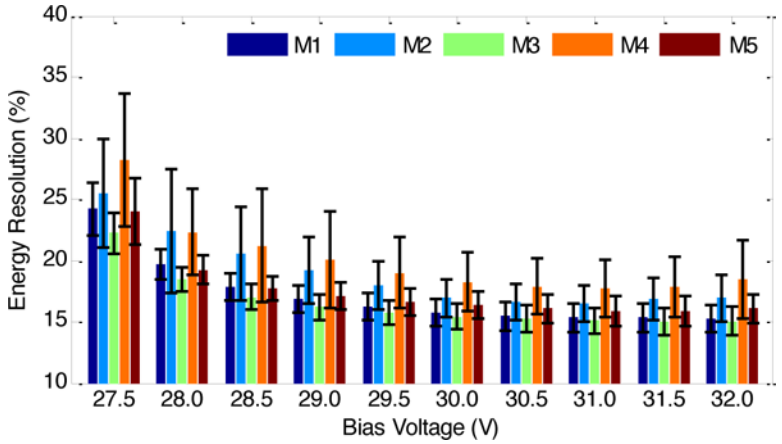

Fig. 9.
Energy resolution versus bias voltage.

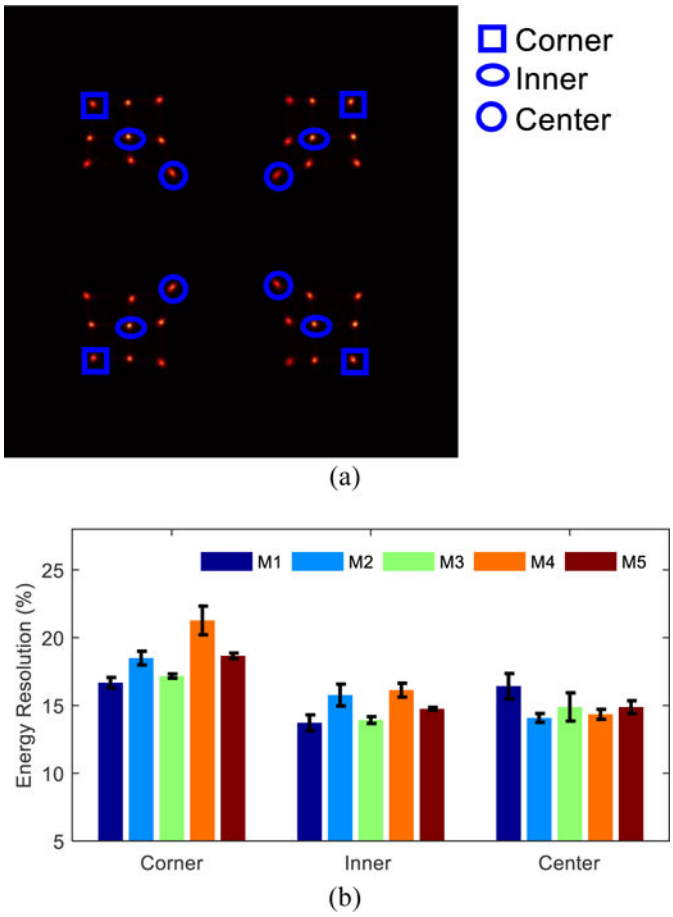

Fig. 10.
(a) Crystal positions and (b) average energy resolution at bias voltage 31.0V.

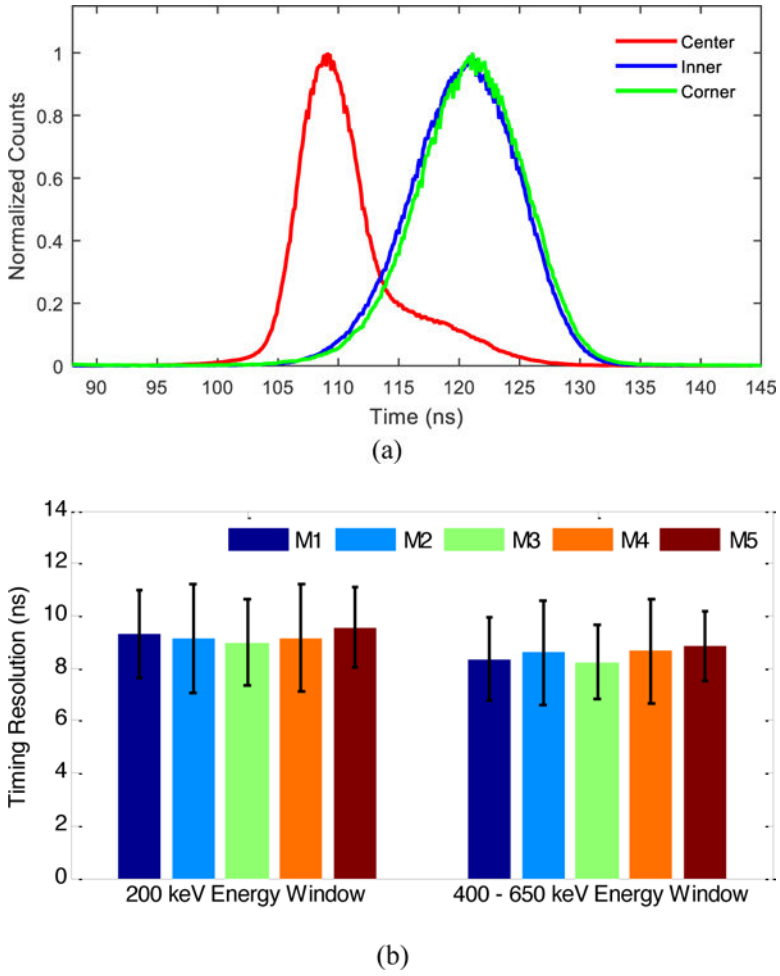

Fig. 11.

(a) Timing spectra using M5 and (b) average timing resolution using different readouts.

Table I

Comparison of the five readout methods[a]

		Readout Method				
		M1	**M2**	**M3**	**M4**	**M5**
Performance	Flood histogram quality	7.3 ± 1.6	4.1 ± 1.7	3.5 ± 0.5	3.9 ± 1.6	3.3 ± 0.4
	Signal-to-noise ratio	33.5 ± 3.1	21.3 ± 1.7	24.6 ± 1.6	17.7 ± 1.3	18.3 ± 1.3
	Energy resolution (%)	15.2 ± 1.2	16.4 ± 1.5	15.0 ± 1.1	17.7 ± 2.3	15.9 ± 1.2
	Timing resolution[b]	8.4 ± 1.6	8.6 ± 2.0	8.2 ± 1.4	8.6 ± 2.0	8.8 ± 1.3
Electronics components[c]	Amplifier[d]	20	24	25	12	5
	Shaper	16	4	4	4	4
	ADC	16	4	4	4	4
	CFD	4	4	1	4	1
	TDC	4	4	1	4	1

[a] Capacitors and resistors are not listed, as they are both used for the multiplexer circuit and filter of power.

[b] 400 – 650 keV energy window was applied to each crystal to select events.

[c] Number are channel number.

[d] One-channel amplifiers are assumed.